J. Fluid Mech. (1992), *vol.* 243, *pp.* 33–50
Printed in Great Britain

The transient response of a contained rotating stratified fluid to impulsively started surface forcing

By G. S. M. SPENCE[1]†, M. R. FOSTER[2] AND P. A. DAVIES[1]

[1] Department of Civil Engineering, The University, Dundee DD1 4HN, UK

[2] Department of Aeronautical and Astronautical Engineering, The Ohio State University, Columbus OH 43210-1275, USA

(Received 13 May 1987 and in revised form 20 January 1992)

The transient response of a contained stratified rapidly rotating fluid to an impulsive surface stress has been studied theoretically and experimentally. The analysis predicts, and the experiments confirm, that for low values of the Burger number S the initial fluid adjustment within the $E^{-\frac{1}{2}}\Omega^{-1}$ timescale is characterized by a barotropic response in which the magnitude of the interior velocity is independent of depth. (Here E and Ω are the Ekman number and rotation rate respectively.) The period of the barotropic response decreases as S increases. For large S, the barotropic flow adjusts subsequently to a baroclinic flow within the $E^{-\frac{1}{2}}\Omega^{-1}$ scale, and during this later stage the excess and deficit in velocity in the lower and upper parts respectively of the fluid are removed. The baroclinic flow forced by the surface stress in these cases is thereby established in a timescale which is typically less than the spin-up time for a homogeneous fluid. The agreement between theory and experiment is shown to be qualitatively good, and the quantitative discrepancies observed between the predicted and measured interior velocities are discussed.

1. Introduction

The transient response of a rotating fluid to an initiation or change in external forcing constitutes a problem of central interest in geo- and astrophysics. The terms 'spin-up' or 'spin-down' have often been employed to describe the response, though these terms have generally been reserved for cases in which the angular velocity of the whole fluid body is either increased or decreased impulsively (see Benton & Clark, 1974, for example, for a comprehensive review of the subject). In such cases, spin-up (down) is held to be the process of adjustment that is initiated when the rotation rate of the fluid is increased (decreased), and completed when the fluid regains solid-body rotation at the new angular velocity. The large body of literature which is available to describe the spin-up phenomenon has substantiated the result that for homogeneous fluids (Greenspan & Howard 1963; Wedemeyer 1964; Weidmann 1976*a*, *b*) the spin-up time is of order $E^{\frac{1}{2}}\Omega^{-1}$, where E is the Ekman number of the flow and Ω is the initial rotation rate of the fluid. For stratified fluids (Holton 1965*a*, *b*; Pedlosky 1967; Walin 1969; Sakurai 1969; Buzyna & Veronis 1971; Hyun 1983), regions of the interior do not reach the new angular velocity until the diffusion time ($O(E^{-1}\Omega^{-1})$) has elapsed, though a quasi-steady state of vertical shear in the interior azimuthal velocity is established in a time less than the homogeneous spin-up time.

In the present study we consider the transient response of a contained rotating

† Present address: Risley Nuclear Power Development Laboratories, Northern Division, UKAEA, Risley, Warrington, Cheshire, WA3 6AT, UK.

linearly stratified fluid to a constant stress applied impulsively to its horizontal upper boundary. As in the previous cases cited above, the initial undisturbed dynamical state of the (cylindrical) fluid body is one of rapid solid-body rotation about a vertical axis. However, here the forcing of the interior is initiated by the differential rotation, ω ($\ll \Omega$), from relative rest of the container's horizontal lid and not by an increase or decrease in the rotation rate of the system.

Previous studies of the present problem have established (Pedlosky 1971; Linden 1977) that the final state of motion in the fluid interior is a steady baroclinic azimuthal flow in which there is a linear vertical shear in the azimuthal velocity. The strength of the shear is determined essentially by the value of the ratio $S/E^{\frac{1}{2}}$, where S is the Burger number of the flow (see below). Since the value of the Ekman number, E, is generally much less than unity for the rapidly rotating flows in question, the viscous timescale ($O(E^{-1})$) in which this final steady state of linear shear is achieved is much longer than the ($O(E^{-\frac{1}{2}})$) Ekman timescale. The principal objective of the present paper is to gain an understanding of the transient behaviour of the fluid within the latter, much shorter timescale. No previous experimental or theoretical investigations of this problem have been made.

2. Formulation of the problem

The flow configuration to be considered is illustrated schematically in figure 1. A cylinder of constant depth H and radius L contains an incompressible linearly stratified, fluid which rotates as a solid body with constant angular velocity Ω about a vertical axis. At time $t = 0$ the horizontal rigid lid of the container is set into motion impulsively, and thereafter maintained with constant angular velocity ω, relative to the rotating cylinder.

Relative to the rotating frame, the momentum, continuity and energy equations governing the subsequent flow of such a fluid may be expressed in the standard form

$$\boldsymbol{q}_t + (\boldsymbol{q}\cdot\boldsymbol{\nabla})\boldsymbol{q} + \boldsymbol{f}\times\boldsymbol{q} = -\rho^{-1}\boldsymbol{\nabla}p - \boldsymbol{g} + \nu\nabla^2\boldsymbol{q}, \tag{2.1}$$

$$\rho_t + \boldsymbol{\nabla}\cdot(\rho\boldsymbol{q}) = 0, \tag{2.2}$$

$$\rho_t + (\boldsymbol{q}\cdot\boldsymbol{\nabla})\rho = \kappa\nabla^2\rho, \tag{2.3}$$

where $\boldsymbol{q} = (u, v, w)$ is the velocity vector in a cylindrical polar coordinate system (r, θ, z), ρ is the density, p is the pressure, $f\hat{\boldsymbol{z}}(= 2\Omega\hat{\boldsymbol{z}})$ is the Coriolis parameter and $\boldsymbol{g} = -g\hat{\boldsymbol{z}}$ is the gravitational acceleration. The kinematic viscosity and mass diffusion coefficient of the fluid are given by ν and κ respectively, with both coefficients being assumed to be constant; the centrifugal acceleration has been neglected.

Attention is restricted to cases in which changes in density are effected solely by varying concentrations of a dissolved solute, so (2.3) has been derived under the assumption that, in the absence of internal heat sources, thermal effects can be neglected.

Exploiting the property that the total pressure and density fields are dominated by their vertical structure, the density field in the absence of relative motion may be expressed as

$$\rho(z) = \rho_{\mathrm{b}} + (\Delta\rho)\,\rho_{\mathrm{s}}(z), \tag{2.4}$$

where ρ_{b} is the density at the base of fluid, and

$$\Delta\rho = \rho_{\mathrm{b}} - \rho_{\mathrm{t}} \tag{2.5}$$

represents the total vertical density difference between the top (t) and bottom (b) of the fluid. To ensure static stability the non-dimensional function $\rho_{\mathrm{s}}(z)$ is negative and monotonic and takes values between 0 and -1.

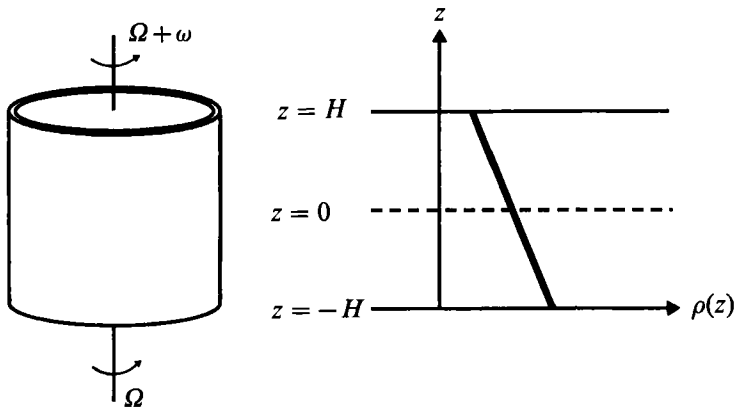

FIGURE. 1. Schematic representation of flow configuration.

The static pressure is defined in a similar manner as

$$p(z) = p_b + p_s(z). \tag{2.6}$$

Equations (2.1)–(2.3) may now be arranged in an appropriate non-dimensional form by non-dimensionalizing all the variables with apposite scale factors, so as to reflect the principal force balance in the flow between the Coriolis and pressure gradient forces (see (2.7)–(2.11) below).

In the following equations the non-dimensional variables are appended with an asterisk to distinguish them from their dimensional forms:

$$(r, \theta, z) = (Lr^*, \theta^*, Hz^*), \tag{2.7}$$

$$(u, v, w) = \omega L(u^*, v^*, \delta w^*), \tag{2.8}$$

$$t = (H/(\nu f)^{\frac{1}{2}})\, t^*, \tag{2.9}$$

$$p(r, \theta, z, t) = p_b + p_s(z) + \rho_b f \omega L^2 p^*(r^*, \theta^*, \zeta^*, t^*), \tag{2.10}$$

$$\rho(r, \theta, z, t) = \rho_b + \Delta\rho[\rho_s^*(z) + Ro\, S^{-1}\rho^*(r^*, \theta^*, z^*, t^*)]. \tag{2.11}$$

In the equations above, H and L are representative vertical and horizontal scales (in this case the half-depth and radius respectively of the fluid container) and the timescale is that for homogeneous spin-up. The scale factor, δ, and the Rossby, Burger and Froude numbers, Ro, S and Fr are defined as

$$\delta = H/L, \tag{2.12}$$

$$Ro = \omega/f, \tag{2.13}$$

$$S = (g\Delta\rho H)/\rho_0 L^2 f^2 = \delta^2 N^2/f^2, \tag{2.14}$$

$$Fr = Ro/S. \tag{2.15}$$

Attention is now confined to the following parameter ranges:

$$E \ll 1, \tag{2.16a}$$

$$Ro = KE^{\frac{1}{2}}, \quad K = O(1), \tag{2.16b}$$

$$S = O(1), \tag{2.16c}$$

$$\delta = H/L = O(1), \tag{2.16d}$$

$$E^{\frac{1}{2}}\delta^2/\sigma = O(1), \tag{2.16e}$$

$$\Lambda \ll E^{\frac{1}{2}}, \tag{2.16f}$$

where $A = \Delta\rho/\rho_0$, and the Ekman number, E, and the Schmidt number σ are given by $E = \nu/fH^2$ and $\sigma = \nu/\kappa$ respectively. These approximations result in the Boussinesq equations:

$$E^{\frac{1}{2}}u_t + Ro[uu_r + wu_z - v^2/r] - v = -p_r + \delta^2 E[\nabla^2 u - u/r^2], \tag{2.17}$$

$$E^{\frac{1}{2}}v_t + Ro[uv_r + wv_z + uv/r] + u = \delta^2 E[\nabla^2 v - v/r^2], \tag{2.18}$$

$$E^{\frac{1}{2}}w_t + Ro[uw_r + ww_z] = -p_z - \rho + \delta^2 E[\nabla^2 w], \tag{2.19}$$

$$r^{-1}(ru)_r + w_z = 0, \tag{2.20}$$

$$E^{\frac{1}{2}}\rho_t + Ro[u\rho_r + w\rho_z] - Sw = E\delta^2\sigma^{-1}(\nabla^2\rho), \tag{2.21}$$

where

$$\nabla^2 = \frac{\partial^2}{\partial r^2} + \frac{1}{r}\frac{\partial}{\partial r} + \frac{\partial^2}{\partial z^2} \tag{2.22}$$

is the three-dimensional Laplacian, and axial symmetry has been assumed.

If it is assumed that the dynamics of the flow are dominated by Ekman pumping-suction, the dependent variables can be expanded in $E^{\frac{1}{2}}$ in the standard manner (Pedlosky 1979) to give the following zeroth-order equations for (2.17)–(2.21):

$$v_0 = p_{0r}, \tag{2.23}$$

$$u_0 = 0, \tag{2.24}$$

$$\rho_0 = -p_{0z}, \tag{2.25}$$

$$r^{-1}(ru_0)_r = -w_{0z}, \tag{2.26}$$

$$w_0 = 0. \tag{2.27}$$

The first-order relations are given by

$$-v_1 - Kv_0^2/r = p_{1r}, \tag{2.28}$$

$$v_{0t} + u_1 = 0, \tag{2.29}$$

$$\rho_1 = -p_{1z}, \tag{2.30}$$

$$r^{-1}(ru_1)_r = -w_{1z}, \tag{2.31}$$

$$\rho_{0t} = Sw_1, \tag{2.32}$$

where the absence of the diffusion term in (2.32) leads to (2.16*e*). (Note that in the above, asterisks have been dropped for convenience.)

Eliminating u_1 and w_1 from (2.29), (2.31) and (2.32) we have an equation involving ρ_0 and v_0, which may then be written entirely in terms of p_0, from (2.23) and (2.25). The result is an equation whose first (simple) time integral gives the elliptic equation for p_0,

$$\nabla_1^2 p_0 + \frac{1}{S}\frac{\partial^2 p_0}{\partial z^2} = 0, \tag{2.33}$$

where ∇_1^2 is the horizontal Laplacian (in our case here, simply given by $r^{-1}\,\partial/\partial r(r\partial/\partial r)$). Thus, the spin-up problem reduces to solving (2.33) subject to appropriate boundary conditions on $z = 1$ and $z = -1$.

2.1. *The boundary conditions*

In the Appendix, we show, following Pedlosky (1967), that for $S = O(1)$, the sidewall boundary layer on $r = 1$ can carry no net vertical flow of fluid, so that layer cannot accept an $O(E^{\frac{1}{3}})$ inflow at its edge (in contrast to the homogeneous case!). Hence, u must be zero at $r = 1$, and, from (2.23) and (2.29), there is the condition

$$\frac{\partial p_0}{\partial r} = 0 \quad \text{on} \quad r = 1 \tag{2.34}$$

on the azimuthal velocity component. It should be pointed out that the velocity no slip is not due to the inability of some boundary layer on $r = 1$ to take that slip velocity to zero; it is rather that the Coriolis force-induced radial velocity connected to the time rate of change of v_0 must vanish at $r = 1$ because of the strong constraints imposed by buoyancy near the wall.

The spin-up discussed here takes place on a timescale long compared with the timescale for the unsteady development of the Ekman layers, so the Ekman-layer dynamics are quasi-steady. An important result from Ekman dynamics is that the radial flux of fluid in such a layer is given by

$$-(1/\sqrt{2})\, E^{\frac{1}{2}}(u_{\mathrm{G}} + v_{\mathrm{G}} - u_{\mathrm{B}} - v_{\mathrm{B}}), \tag{2.35}$$

where the subscript G denotes components in the geostrophic flow at the edge of the Ekman layer, and the B subscript identifies velocities at the boundary. Hence, under (2.24), the volumetric flow rate into the upper corner is given by the product of the flux and the flow area, i.e.

$$\sqrt{2}\pi E^{\frac{1}{3}}. \tag{2.36}$$

Now, in a homogeneous case, this fluid enters the Stewartson $E^{\frac{1}{3}}$ layer, flows down, then radially outward into the fluid interior, pushing ahead of it spun-up fluid. As we have noted already, there is no shear layer in this rotating stratified fluid capable of accepting a fluid flow rate of this magnitude. Therefore, this fluid flows into the corner, and erupts into the interior as a source. Since the flow rate is $O(E^{\frac{1}{3}})$, that effect translates into a boundary condition on w_1, i.e.

$$w_1 = -\Phi(r-1)\sqrt{2} \quad \text{on} \quad z = 1, \tag{2.37a}$$

where $\Phi(x-x_0)$ denotes the Dirac delta function with singularity at x_0. Now, the Ekman velocity compatibility condition to be applied on the outer flow at the horizontal boundaries is given in our notation by

$$w = \pm(1/\sqrt{2})\, E^{\frac{1}{2}}(\zeta_{\mathrm{B}} - \zeta) \quad \text{on} \quad z = \pm 1, \tag{2.37b}$$

with the vorticity component $\hat{\boldsymbol{z}} \cdot \nabla \times \boldsymbol{q}$ denoted by ζ. Substitution of the $E^{\frac{1}{2}}$ expansion into this equation gives the compatible vertical velocities at the boundaries

$$w_1 = (1/\sqrt{2})\,(2 - \nabla_1^2 p_0)\,(1/\sqrt{2})\,\Phi(r-1) \quad \text{on} \quad z = 1, \tag{2.38a}$$

$$w_1 = (1/\sqrt{2})\,\nabla_1^2 p_0 \quad \text{on} \quad z = -1, \tag{2.38b}$$

where we have appended to the boundary condition obtained from the Ekman conditions the requirement of mass conservation, (2.37*a*). Now, recall that w_1 is given in terms of p_0 by (2.32). Substitution gives the boundary conditions for (2.33),

$$\frac{\sqrt{2}}{S}\frac{\partial p_0^2}{\partial z\, \partial t} = \nabla_1^2 p_0 - 2 + \Phi(r-1) \quad \text{on} \quad z = 1, \tag{2.39a}$$

$$\frac{\sqrt{2}}{S}\frac{\partial^2 p_0}{\partial z\, \partial t} - \nabla_1^2 p_0 \quad \text{on} \quad z = -1. \tag{2.39b}$$

So, the initial-value problem is posed as the solution of (2.33) with (2.35) and (2.39). We proceed now to the solution.

2.2. *The exact solution*

We seek solution to (2.33) and (2.39) in the form

$$p_0 = \sum_{n=1}^{\infty} A_n(z,t)\, J_0(\alpha_n r), \tag{2.40}$$

where, to satisfy (2.34) on $r = 1$, $\{\alpha_n\}$ are the zeros of the J_1 Bessel function. Substitution of this solution into (2.32) leads to the equation for A_n,

$$\frac{1}{S}\frac{\partial^2 A_n}{\partial z^2} - \alpha_n^2 A_n = 0, \tag{2.41}$$

and the boundary conditions (2.38) become

$$\left(\frac{\partial^2 A_n}{\partial z\,\partial t}\right) + \frac{1}{\sqrt{2}}\left(\frac{\partial^2 A_n}{\partial z^2}\right) = B_n, \quad z = 1, \tag{2.42a}$$

$$\left(\frac{\partial^2 A_n}{\partial z\,\partial t}\right) + \frac{1}{\sqrt{2}}\left(\frac{\partial^2 A_n}{\partial z^2}\right) = 0, \quad z = -1, \tag{2.42b}$$

with

$$B_n = \frac{S}{\sqrt{2}} \frac{\int_0^1 [\Phi(r-1)-2]\, r J_0(\alpha_n r)\, \mathrm{d}r}{\int_0^1 r[J_0(\alpha_n r)]^2\, \mathrm{d}r}, \tag{2.42c}$$

where B_n may be evaluated, and gives simply $-S\alpha_n r_n/\sqrt{2}$ with r_n the Fourier-Bessel J series expansion for r, so

$$r_n 2/[\alpha_n J_2(\alpha_n)]. \tag{2.42d}$$

Equation (2.41) may then be solved under (2.42) by separation of variables or Laplace transformation. In any case, the solution for the swirl, v_0, is given by

$$v_0 = \frac{1}{2}\sum_{n-1}^{\infty} r_n \left[\frac{\cosh(m_n z)}{\cosh(m_n)}(1-\exp(-j_n t)) + \frac{\sinh(m_n z)}{\sinh(m_n)}(1-\exp(-h_n t))\right] J_1(\alpha_n r), \tag{2.43}$$

with the parameters in the solution given as

$$m_n = S^{\frac{1}{2}}\alpha_n, \quad h_n = (m_n/\sqrt{2})\tanh(m_n), \quad j_n = (m_n/\sqrt{2})\coth(m_n). \tag{2.44a–c}$$

Notice that, for time large, the exponentials in (2.43) vanish, and the solution approaches a solution of the steady equation. For extreme values of S, we can make the following approximations.

$S \ll 1$: for $S \to 0$ (meaning small effects of stratification), notice that $m_n \to 0$ for all finite α_n, so that $h_n \to O(s)$, and $j_n \to 1/\sqrt{2}$. Hence, (2.43) may be summed approximately, and we have

$$v_0 \sim \tfrac{1}{2}r(1-\exp(-t/\sqrt{2})) + O(S) + z\sum_{n=1}^{\infty} r_n(1-\exp(-\alpha_n^2 St/\sqrt{2}))\, J_1(\alpha_n r), \quad S \ll 1. \tag{2.45}$$

Of course, for α_n of order $S^{-\frac{1}{2}}$ or larger, $m_n = O(1)$ and so large-n terms in the series do not lead to forms like those in (2.45); but, $r_n = O(S)$ for those cases, so they make

very small alterations to the (2.45) result, and are accounted for by the '$O(S)$' notation. It is also clear from (2.45) that $S \to 0$, $t \to \infty$ are non-commutative. If $t = O(1)$, then the entire second term is $O(S)$, indicating that on the spin-up timescale, the spin-up is just like the homogeneous case. However, for $t = O(1/S)$, each Fourier mode spins up with a linear shear in the vertical, and further, for $St \gg 1$, the exponential is small and so (2.45) becomes

$$v_0 \sim \tfrac{1}{2}r(1+z), \quad t \to \infty. \tag{2.46a}$$

It is worth noting that this $1/S$ timescale is immediately evident from (2.39) itself. There are great complexities in this small-S case not evident in what we have just done; further details may be found in the Appendix. What *is* clear from (2.33), and more opaque in (2.43) is that if $S \ll 1$, then the solution includes a thin $S^{\frac{1}{2}}$ layer inside $r = 1$. We examine that region by writing $r = 1 + S^{\frac{1}{2}}\xi$; then, the argument of the Bessel function in (2.43) becomes $\alpha_n + m_n \xi$. Letting S go to zero in this expression recovers (2.45) evaluated at $r = 1$, unless we take m_n to be $O(1)$ for $S \to 0$. From (2.44a) for that to be so, α_n must be large; hence, we see that the large-n terms in the series are important to the structure near the wall, as we would expect, since large-n Bessel functions have small-scale radial structure. Since m_n is $O(1)$, then (2.43) and (2.44b, c) indicate that, in fact, the structure in this layer is much more complex than the simple (2.45) solution, since h_n and j_n are $O(1)$ and, hence, there is significant z-structure as well. So, in small-S spin-up, the baroclinic effects are confined to this $S^{\frac{1}{2}}$ layer. Thus, one restriction on (2.45) and (2.46a) is

$$r - 1 \gg S^{\frac{1}{2}}. \tag{2.46b}$$

It is now well understood that (2.45) fails on a diffusion timescale, so that '$t \to \infty$' means in fact t large, but $t \ll E^{-\frac{1}{2}}$. However, we show in the Appendix that the (2.43) solution fails for S small unless

$$t \ll S/E^{\frac{1}{2}}, \tag{2.46c}$$

so, quite evidently, the solution given here makes no sense unless, S, though small, is large compared to $E^{\frac{1}{2}}$. Therefore, the most severe restriction on (2.46a) is (2.46c) and

$$S \gg E^{\frac{1}{2}}, \tag{2.46d}$$

Further, the entire analysis given here is predicated on the fact that the 'buoyancy layer' on the $r = 1$ surface can accommodate no falling fluid, hence the corner singularity expressed in (2.38a). As the Appendix shows, that buoyancy layer merges with a Stewartson '$\frac{1}{3}$-layer' if S is as small as $(E\delta^2)^{\frac{2}{3}}/\sigma$. Now, for S larger than this value but smaller than $E^{\frac{1}{2}}$, the outer layer changes structure slightly, but remains the layer which absorbs the corner flow, so we expect the overall structure to be not very different. However, below $(E\delta^2)^{\frac{2}{3}}/\sigma$, fluid flows down the wall, and the outer-layer structure changes significantly.

Having noted that, however, it should be pointed out that the core fluid always spins up in the same fashion – Ekman pumping in and out of the horizontal layers, and fluid fed into the interior by the layers on $r = 1$. So, whatever the complexities of the wall layers, the small-S core flow seems unaffected for $t = O(1)$.

For completeness, we note additionally that (2.33) is only the proper interior differential equation for times of order $1/S$ if S is much larger than $O(E^{\frac{1}{2}}\delta^2/\sigma$; for S values that are comparable to that value or smaller, density diffusion becomes important throughout the interior of the flow. In general, the details of the small-S structure, as discussed further in the Appendix as well, are far too involved for treatment in this paper and await further work.

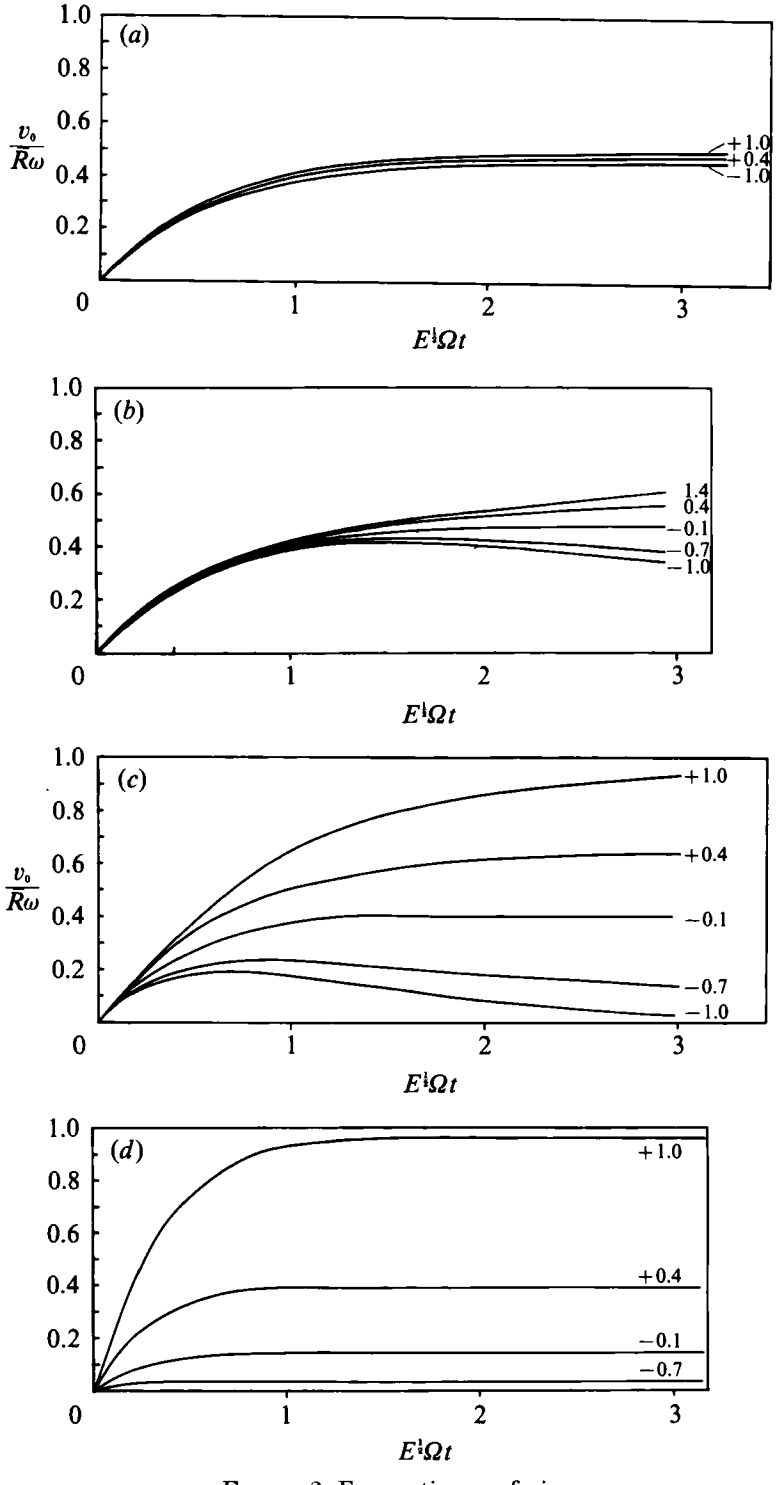

FIGURE 2. For caption see facing page.

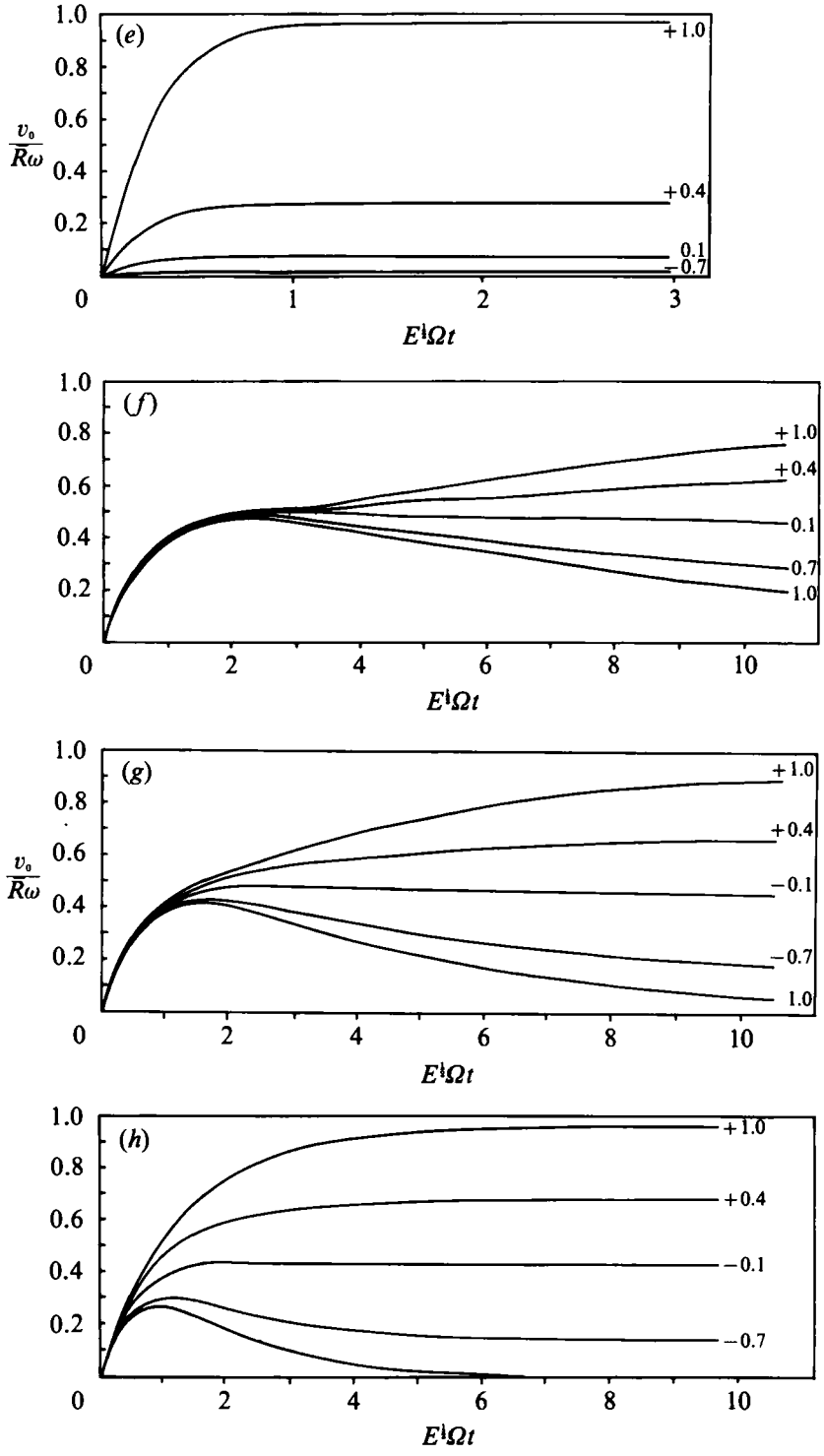

FIGURE 2. Plots of non-dimensional azimuthal velocity v_0 (non-dimensionalized with the lid velocity at mid-radius, $\bar{R}$) against time (non-dimensionalized by $E^{-\frac{1}{2}}\Omega^{-1}$), for $Ro = 1.38 \times 10^{-2}$, $E = 1.28 \times 10^{-4}$, $\delta = 0.27$ and $z/H = 1.0$, 0.4, -0.1, -0.7 and -1.0, as indicated on the curves (*a*) $S = 0.001$, (*b*) $S = 0.01$, (*c*) $S = 0.05$; (*d*) $S = 0.29$; (*e*) $S = 0.5$; (*f*) $S = 0.005$; (*g*) $S = 0.01$; (*h*) $S = 0.03$.

$S \gg 1$: for S large, on the other hand, it is evident from (2.44a) that all of the m_n are large, regardless of n, hence both h_n and j_n are asymptotic to $(\frac{1}{2}S)^{\frac{1}{2}}\alpha_n$. The ratios of hyperbolic functions in (2.43) are approximated by exponentials, and hence, to leading order, (2.43) becomes

$$v_0 \sim r_1 \exp[S^{\frac{1}{2}}\alpha_1(z-1)]\, J_1(\alpha_1 r)\,(1-\exp[-\alpha_1(\tfrac{1}{2}S/2)\,t]), \quad S \gg 1, \tag{2.47}$$

from which it is evident that the decay toward a steady state takes place on a timescale $S^{-\frac{1}{2}}$ rather than $O(1)$ or $O(S^{-1})$, and further that the bulk of the fluid does not spin up – rather, the spinning fluid is all contained in a 'penetration depth' region of width $S^{-\frac{1}{2}}$ near the upper boundary, and in particular

$$v_0 \to r_1 \exp[S^{\frac{1}{2}}\alpha_1(z-1)]\, J_1(\alpha_1 r), \quad t \to \infty \quad \text{and } S \text{ large}. \tag{2.48}$$

(There are an infinite number of terms like the r_1 term given in (2.47) and (2.48); however, all other terms are order $\exp(-S^{\frac{1}{2}})$ smaller than the first, and hence play a transcendentally small role in the large-S solution.)

Finally, it is in order to notice, from the general solution (2.43) for arbitrary S, that $v_0 \to 0$ for $t \to \infty$ on $z = -1$, and that $v_0 \to r$ for $t \to \infty$ on $z = +1$, so that the fluid in the neighbourhoods of each of those boundaries moves with the speed of the boundaries. The distribution of that azimuthal speed with height, then, varies from linear variation for S small, to exponential variation near $z = 1$ for S large.

3. Numerical results

The series (2.42) was evaluated numerically to give values of the azimuthal velocity v_0 and its variation with time at mid-radius ($r = \bar{R}$) and various depths in the flow. Some of the results of the computations are shown in figure 2. In all graphs the ordinates and abscissae have been normalized by the tangential lid velocity at mid-radius and the Ekman timescale respectively.

3.1. *Variation of flow behaviour with S*

At the smallest value of S (see figure 2a) the flow behaviour resembles closely that of a homogeneous ($S = 0$) fluid, with the azimuthal velocity v_0 exhibiting height-independence and an asymptotic increase with time to a value half that of the lid. The Taylor–Proudman two-dimensionality constraint shown in figure 2a is not broken until values of S close to $S = 0.01$ are attained (see figure 2b), and, even for this value of S, the tendency of the fluid to behave in a manner resembling that of a homogeneous fluid remains strong in the early stages of the response. In particular, there is a well-defined initial barotropic response. The flow does not display baroclinic behaviour (i.e. a splitting into individual responses for each level) until approximately one Ekman period has elapsed after the initiation of lid motion. At and around the value of $S = 0.01$, the description of the spin-up process ceases to have the accepted significance, as the interior velocity field is subject to large variation with height on timescales long in comparison to the Ekman $E^{\frac{1}{2}}$ spin-up timescale.

Figure 2(c) demonstrates that stratification has become the dominating influence at $S = 0.05$. As $z/H \to 1$ the flow velocity increases relatively slowly and monotonically to approach the lid velocity at large times, while fluid at mid-depth spins up (i.e. approaches to within 1/e of its asymptotic velocity) the most rapidly, with the initial barotropic response aiding this behaviour. Overshoot in velocity is clearly evident in the lower levels of the fluid, with the excess angular velocity here being removed over approximately four $E^{-\frac{1}{2}}$ spin-up times.

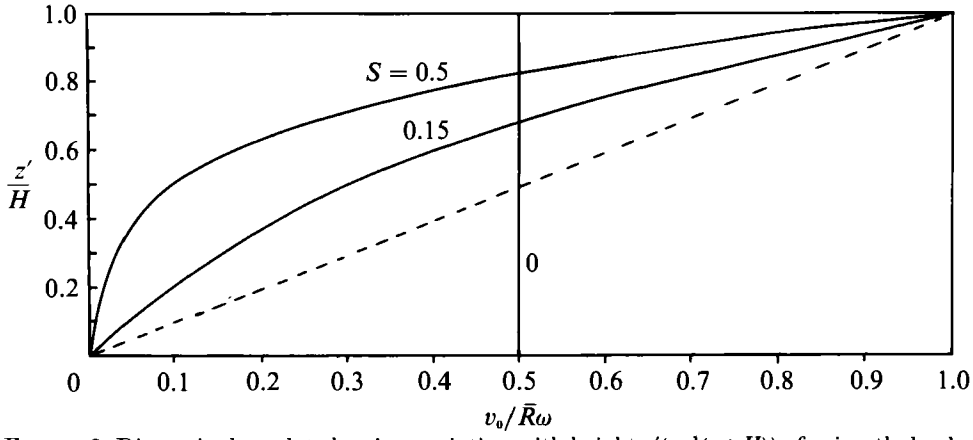

FIGURE 3. Dimensionless plot showing variation with height $z'(=\frac{1}{2}(z+H))$ of azimuthal velocity at mid-radius $\bar{R}$, 8 min (8.17 ω^{-1} advection time units) after initiation of impulsive surface forcing. Values of Ro, E, δ as for figure 2. For reference theoretical homogeneous (S = 0) profile ($v_0/\bar{R}\omega = 0.5$) also indicated.

As S increases successively in value (see figure 2*a–c*) the Taylor–Proudman constraint of two-dimensional flow is broken more rapidly and the length of time over which the barotropic adjustment operates is shortened. Consequently, as S increases, fluid in the lower levels does not gain achieve such large initial velocities, and the overshoot phenomenon becomes progressively less evident. Inhibition of the spin-up dynamics at large depth continues with increasing values of S (as revealed by inspection of figures 2*d*, *e*) and for values of $S = 0.29$ and above, the initial response is seen also to be baroclinic. Indeed, for the value $S = 0.5$ (see figure 2*e*) buoyancy effects so inhibit the vertical Ekman pumping that fluid at large depths is not affected significantly by lid motion. In accordance with the findings of Walin (1969) and Sakurai (1969), and consistent with our results in (2.47), the spin-up process is confined to the region in the vicinity of the lid at large values of S, and the adjustment is more rapid than that in the analogous homogeneous spin-up process – compare, for example, figures 2(*a*) and 2(e).

It is possible to examine the long-term behaviour of low-S-value flows (see figure 2*f–h*) if it is presumed that the vorticity equation (2.32) remains valid for times in excess of ten Ekman $E^{-\frac{1}{2}}$ spin-up periods. For the case $S = 0.001$ (not shown) the flow retains the homogeneous character shown by figure 2(*b*), for times in excess of ten Ekman spin-up periods, but as the value of S increases from 0.005 through 0.01 to 0.03, the overshoot in the lower part of the fluid becomes progressively less marked. In consequence, the interior velocity of the fluid near the bottom of the container is reduced to zero more rapidly than for low-S cases by the action of the Ekman layer activated on the lower solid boundary soon after the lid motion commences. It is of interest to note that the dynamics of the weakly stratified rotating flows are extremely sensitive to the values of S under consideration. This general behaviour has been observed in other contexts (Davies, 1972; Davies, Davis & Foster 1990) where the presence of slight stratification has been shown to be sufficient to change the flow structure dramatically from that occurring with the homogeneous case. In the present configuration, the phenomenon is well illustrated by figure 3 where a comparison of flow profiles is made for various values of S, including $S = 0$. Note, in particular, the dramatic difference between the homogeneous ($S = 0$) and stratified cases, and the relatively modest changes which occur at higher values of S ($S > 0.1$).

It would be noted that the predictions of theory at very low S values must be treated with caution since the $S = O(1)$ scaling relation (2.16c) employed in the derivation of the governing equation is strictly invalid for these cases. However, the recovery of a stable homogeneous solution at values of $S \lesssim 0.001$ does indicate that the $S = O(1)$ restriction is weak and may therefore be relaxed.

4. Comparison with laboratory experiments

In order to investigate further the transient effects described above, a number of laboratory experiments were conducted in the same parameter range as the theoretical model. The linearly stratified fluid was contained in a circular Plexiglas cylinder of total depth 30 cm and radius 30 cm, mounted on a variable-speed rotating turntable. A rigid horizontal, Plexiglas lid, supported on dry bearings on a central cylindrical column of radius 4 cm, could be rotated differentially with respect to the rest of the container by means of a separate variable-speed motor. A false base, made from Plexiglas, was supported on four sectional pillars, the lengths of which could be varied to allow the working depth to be increased or decreased. The fluid was stratified with salt and fresh water, using the Oster double-reservoir technique, and the initial density profile within the container was measured with a miniature conductivity probe mounted on a vertical traverse support. A gap of approximately 5 mm was left between the rim of the lid and the inner surface of the cylinder wall. The flow at various depths in the fluid was visualized by releasing dye electrolytically (Honji, Taneda & Tatsuno 1980; Boyer & Davies 1982) from an array of thin wires stretched horizontally across the fluid, and illuminating individual levels with a thin slice of light from a projector mounted on the rotating table. The positions of the dye lines were recorded photographically, and the angular displacements of the lines in a given interval were measured to give values of the azimuthal velocity $v_0(z, t)$ at any radial location.

As indicated above, the flow in the configuration under consideration is baroclinically unstable when, for constant E, S and H/L, the Rossby number exceeds a critical value (Linden 1977; Spence 1986). The present spin-up study was restricted to flows which were stable. In general, for such flows, the radial dependence of the azimuthal velocity was observed to be linear up to and beyond mid-radius: however, during, and for some time subsequent to the completion of, the spin-up process, dye lines at different heights within the fluid displayed markedly disparate behaviour at larger radii. At these locations, dye lines in the lower levels of the fluid were retarded with respect to a linear radial velocity profile, whilst those lines at greater elevations showed acceleration.

For nearly all of the experiments conducted, the effect of the impulsive lid start could be observed to varying degrees at all depths (see below). Exceptions to this rule occurred in a number of experiments which were conducted in a tank of large depth containing a strongly stratified fluid. In these cases, with low values of ω and Ω, it was observed that the spin-up dynamics did not extend from the lid throughout the entire depth of the container. In this respect, the observations were in qualitative agreement with the notion of a penetration depth (Walin 1969) of $S^{-\frac{1}{2}}H$, also evident in (2.47), below which the spin-up dynamics do not operate.

For low values of S ($S < 0.01$) the initial response of the fluid was observed to be barotropic, as indicated by dye lines at all heights moving off together with the same azimuthal velocity. Flows with S values in excess of 0.05 also displayed an initial barotropic response, but for a period determined by the degree of stratification. At

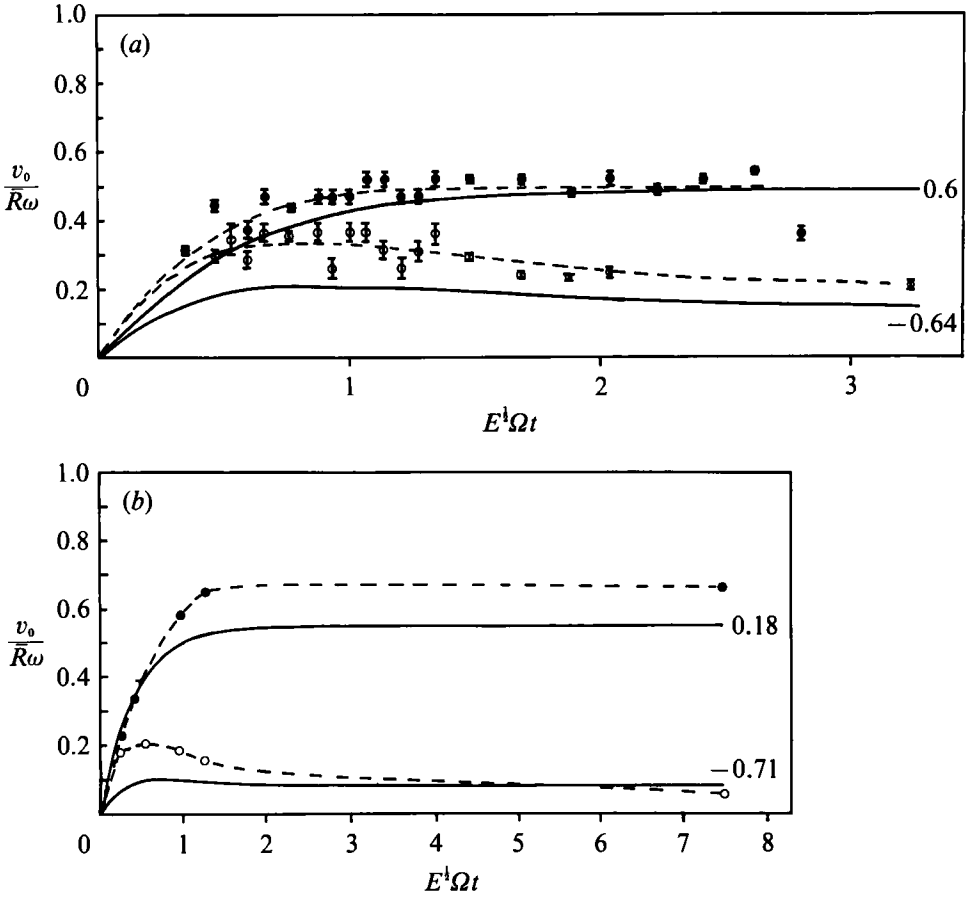

FIGURE 4. Comparison of theoretical (———) and experimental (– – – – –) variation of $v_0/\bar{R}\omega$ with time (non-dimensionalized as in figure 2) for (*a*) $S = 0.06$, $z/H = 0.06$ and -0.64; and (*b*) $S = 0.14$, $z/H = 0.18$ and -0.71 (experimental errors are less than the resolution of the graph and have therefore been omitted). Other parameters as for figure 2.

higher values of S the period of the baroclinic response was weakly dependent upon the value of S. In particular, the appearance of relative separation between dye lines at different heights, which indicated the entry of baroclinic modes into the velocity field, occurred more rapidly with increasing S. However, for lower values of the Burger number ($S < 0.01$) the barotropic response was protracted and its duration was strongly dependent upon the numerical value of S. As a result of this barotropic response for small and moderate values of S, there existed an excess of angular velocity in the lower levels of the fluid and a deficit in the upper levels soon after the initiation of the lid motion. Over a period of several ($O(E^{-\frac{1}{2}})$) spin-up times these excess and deficit velocities were removed by a temporarily activated lower Ekman layer, and a permanent upper Ekman layer respectively, to leave an azimuthal velocity field which varied with height. The results of two sets of experiments with $S = 0.06$ and 0.14 are shown in figures 4(*a*) and 4*b* respectively. In each figure, a comparison is shown with the corresponding analytical solution for the same parameter values. In both figures the presence of an overshoot in velocity in the deeper regions of the fluid is clearly seen.

For the case of $S = 0.06$, results are presented for the azimuthal velocities at

dimensionless heights $z = +0.06$ and -0.64, and it can be seen that at the latter level, for both theory and experiment, the peak of the overshoot occurs after approximately 0.75 Ekman spin-up times, although the theory underestimates the strength of the overshoot. This quantitative lack of accord between theoretical prediction and observation was common to all cases examined. At the greater height of $z = +0.06$ the agreement between experiment and theory is closer, and within experimental error after about one Ekman period. However, the velocity is consistently underestimated in the initial interval. The quantitative correlation between theory and experiment improves with increasing height for all cases examined and the long-term value of the azimuthal velocity is predicted to within experimental error at higher levels. Discrepancies between prediction and observation are more pronounced for the case $S = 0.14$, though there are fewer data points available for comparison. Quantitative agreement is fair for this case, with overshoot at lower levels clearly evident in the experimental data set.

The evidence of the theoretical and experimental results above indicates that the transient response of the fluid to impulsive surface forcing occurs in three stages, as with the homogeneous and stratified spin-up cases studied previously. (For the configuration under investigation in the present study, the dimensional timescales of importance are 1.6 s (Ω^{-1}), 145 s ($E^{-\frac{1}{2}}\Omega^{-1}$) and 12800 s ($E^{-1}\Omega^{-1}$)).

The spin-up process is initiated at a time $t = 0$, when the lid is set impulsively into motion, rotating differentially at a pre-determined speed relative to the other solid surfaces of the container. Rayleigh shear layers develop immediately on horizontal surfaces, becoming quasi-steady Ekman layers within approximately one revolution (Greenspan 1968). Fluid within the Ekman layer adjacent to the lid flows radially outwards, with continuity requiring that replacement fluid be drawn in from the inviscid interior. During this phase the fluid responds in the same way as in the familiar spin-up process for the case where the rotation rate of the whole container is increased.

The action of the Ekman layers is strong following the impulsive start of differential rotation, when the vorticity of the interior fluid adjacent to the upper Ekman layer differs greatly from that of the fluid immediately adjacent to the lid. During and subsequent to this period, fluid is drawn upwards into the upper Ekman layer: in the process, such fluid acquires increased angular velocity, and returns to the interior from the erupting Ekman layer in the upper corner of the flow domain.

In the inviscid interior, fluid which is drawn in from large radius to replace that drawn up to the upper Ekman layer, acquires increased angular velocity through conservation of angular momentum, in a similar manner to the homogeneous spin-up process (Greenspan 1968). During the initial barotropic response for small-S cases, fluid at large depths acquires greater angular velocity than that corresponding to the steady profile remaining at the conclusion of the spin-up process. In consequence, that part of the flow passing adjacent to the lower boundary causes an Ekman layer to form on the solid surface. This layer then acts to remove the excess velocity in the lower levels of the fluid.

Fluid moving radially outward within the upper Ekman layer reaches the vicinity of the corner region (the region of overlap between the Ekman and vertical boundary layers), where, owing to the insulating nature of the container, the sidewall boundary layers are unable to accept the flux from the Ekman layer (see Pedlosky 1967, and the Appendix). Consequently, an intense jet leaves the Ekman layer at this point (Walin 1969) and upper interior fluid in the vicinity of the sidewalls receives a concentrated flux of high angular velocity fluid (see figure 5).

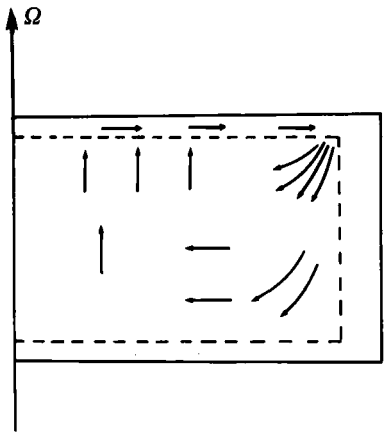

FIGURE 5. Schematic representation of the meridional circulation within the fluid following the onset of differential rotation, ω.

If lower-level fluid were to move radially inwards, and increase the angular velocity of the inner regions by conservation of angular momentum, it could only be replaced with fluid from either the lower Ekman layer or the vertical sidewall boundary layers. However, the lower Ekman layer cannot be activated until the relative vorticity of the region adjacent to it differs from that of the boundary. Moreover, when activated, it pumps fluid upwards so as to reduce the low-level angular velocity. In addition, the motion of deep fluid from the sidewall is prohibited owing to the insulating nature of the vertical boundaries (Pedlosky 1967; Sakurai 1969). In consequence, a region of stagnant fluid is formed at high-radius locations in the deepest regions of the container. In contrast to the above, upper-level fluid at mid-radius is replaced by fluid descending from greater height and large radius, in the manner shown in figure 5.

It may be noted in passing that Buzyna & Veronis (1971) have explained the disparate appearance of dye lines at large radius in terms of radial diffusion of momentum from the sidewalls (although this is not applicable to the present arrangement, where the velocity of the sidewalls remains constant throughout the experiment). Buzyna & Veronis corrected Walin's inviscid interior solutions near $r = 1$, by the *a posteriori* addition of a complementary error function. However, this is not a function of the vertical coordinate and is therefore incapable, alone, of describing differences in near-wall behaviour at various heights. Reference to Buzyna & Veronis' data shows that although excellent accord is found between their experiment and Walin's theory with radial diffusion added, the original theory itself predicts regions of accelerated and decelerated flow. It seems, therefore, that the phenomenon cannot be attributed entirely to radial diffusive effects.

Conclusion of the spin-up process occurs as the interior fluid adjacent to the horizontal boundaries acquires the vorticity of the container, and the vertical velocities driven by the Ekman layers decay asymptotically to zero. Subsequent alterations to the interior velocity profile are effected by the direct action of viscous forces on the much longer dimensional timescale of $t = E^{-1}\Omega^{-1}$.

The authors are pleased to acknowledge the financial support of the Natural Environment Research Council (through a studentship award to G.S.M.S.), NATO Scientific Affairs Division, the UK Science and Engineering Research Council, and

the Carnegie Trust for the Universities of Scotland. Further, they are grateful for the technical assistance and advice of Mr D. E. Moser and Mr E. Kuperus in the experimental programme. The authors derived great benefit from fruitful discussions with Professors D. L. Boyer and G. J. F. van Heijst; the contributions of each are gratefully acknowledged.

Appendix

The analysis in this paper assumes that the azimuthal fluid velocity component v does not slip over the peripheral boundary $r = 1$, whereas in the homogeneous case, the core flow slips over the surface. The reason for the difference is explained in the boundary-layer analysis below, and discussed more intuitively at the end of this section. The analysis of Pedlosky (1967) is relevant to this point, and will not be repeated here in its entirety; as he points out, on $r = 1$ there is an $E^{\frac{1}{2}}$ layer, analogous to the Ekman Layer – a 'buoyancy layer' – whose equations are easily put into the form

$$\frac{\partial^2 \chi}{\partial \xi^2} - 2\mathrm{i}\chi = -2i\chi_{\mathrm{E}}, \quad \chi = \rho + (\sigma S)^{\frac{1}{2}}\mathrm{i}w \tag{A 1}$$

and the boundary-layer coordinate ξ is defined by $\xi = (r-1)/(2E\delta^2(\sigma S)^{\frac{1}{2}})^{\frac{1}{2}}$. Integrating this equation across the layer, then taking the real part gives

$$\frac{\partial \rho}{\partial \xi} = -2(\sigma S)^{\frac{1}{2}} \int_{-\infty}^{0} w \, \mathrm{d}\xi \tag{A 2}$$

which makes the point that, if the density obeys a no-flux condition at the vertical boundary, $r = 1$, then the $E^{\frac{1}{2}}$ layer can carry no vertical flux. Hence, all of the Ekman fluid flowing into the corner at $r = 1$, $z = 1$ must erupt into the interior; it cannot flow down the wall in the buoyancy layer. Thus, the condition given as (2.43a) is correct for this insulating condition. For salt-stratified fluid as in the experiments, this requires that the salt be not deposited on the wall. Thus, there can be no radial inflow into the layer, and hence $u_1 = v_0 = 0$ at $r = 1$.

If, on the other hand, the wall density, denoted by ρ_{W} is somehow specified, then the solution for χ is

$$\rho + \mathrm{i}(\sigma S)^{\frac{1}{2}} w = \rho_{\mathrm{E}} + (\rho_{\mathrm{W}} - \rho_{\mathrm{E}})\, \mathrm{e}^{(1+\mathrm{i})\xi}, \tag{A 3}$$

from which it is clear that the vertical volumetric flow rate is

$$\int_{-\infty}^{0} w \, \mathrm{d}\xi = \frac{1}{2(\sigma S)^{\frac{1}{2}}} (\rho_{\mathrm{E}} - \rho_{\mathrm{W}}), \tag{A 4}$$

and fluid may indeed flow down the wall at $r = 1$. Utilizing the continuity equation, and matching to u_1 in the interior solutions, we have the boundary condition

$$\frac{\partial^2 p_0}{\partial r \, \partial t} = \frac{\delta}{(2\sigma^3 S^3)^{\frac{1}{2}}} \frac{\partial^2 p_0}{\partial z^2} \quad \text{at} \quad r = 1. \tag{A 5}$$

Now, the complete solution for the case when $\delta = O(1)$ and $\sigma = O(1)$ is a complex question. The Ekman flux into the corner ($r = 1, z = 1$) is as noted already, but it is clear from (A 4) that there is vertical flux into the same corner (and into the corner at $(1, -1)$) that is also non-zero, depending on the value of $\partial p_0/\partial z$ at $(1, 1)$ and $(1, -1)$. In addition, from (A 5), radial flux is also present all along the vertical extent of the

outer wall. Detailed spin-up results for this case will be presented in a subsequent paper. However, here, if $\sigma S \gg 1$, then (A 5) is approximated by $\partial p/\partial r = 0$ on $r = 1$, the same as for the no-flux condition.

In summary, then, we conclude that the theoretical results presented in this paper are correct if either of the following conditions hold:

$$\partial\rho/\partial r = 0 \quad \text{at} \quad r = 1 \quad \text{or} \quad S\sigma \gg 1. \tag{A 6}$$

and either one leads to the boundary condition on the outer flow,

$$\partial p_0/\partial r = 0 \quad \text{on} \quad r = 1. \tag{A 7}$$

Another way of understanding this result is to suppose that v_0 did not vanish at $r = 1$. Then, from (2.29), u_1 is non-zero there, so there is a volumetric inflow of order $E^{\frac{1}{2}}$ into the sidewall boundary layers. In the homogeneous case, that fluid flows into the $E^{\frac{1}{4}}$ layer and ultimately into the $E^{\frac{1}{3}}$ layer; here, however, since the layer is of width $E^{\frac{1}{2}}$, continuity demands that w be of order one. However, we have seen that the buoyancy-layer structure precludes such a velocity that carries any net mass. Hence, $u_1 = 0$ and hence $v_0 = 0$ on $r = 1$ is the only possibility.

The $S \ll 1$ boundary layers

For $S = O(1)$, the swirling fluid adheres to the outer surface, with a boundary layer – the buoyancy layer – on the vertical velocity. As S gets small, the 'core' solution splits into a central region which is essentially like the homogeneous case (see 2.45)) so long as $t = O(1)$, and a sidewall layer of width $S^{\frac{1}{2}}$ – as noted in §2 of the text. Now, examination of the exact solution or asymptotic analysis for small S shows that the fluid injected into the 'interior' from the Ekman-layer eruption at (1, 1) comes into this $S^{\frac{1}{2}}$ layer. In this region, that fluid flows partly into Ekman layers and partly back into the interior, providing an inflow for the u_1 interior motion – just as in the homogeneous case. Further, also as in the homogeneous case, the swirl velocity, v, slips along the edge of this sidewall layer, so that to the core flow, there is azimuthal velocity slip at its 'wall'. The difference, of course, is that the slip occurs across the $S^{\frac{1}{2}}$ layer here, and across the $E^{\frac{1}{4}}$ layer in the homogeneous case. This picture of the flow fails at some small value of S to be discussed below, and various other structures become important at the wall. Never, however, does the overall $S \ll 1$ flow picture significantly change on this timescale insofar as the core motion is concerned.

If we examine the equations of motion near $r = 1$ in a layer thicker than the buoyancy layer, we find that the most general boundary-layer equation seems to be

$$\frac{\partial}{\partial t}\left(\frac{\partial^2 p}{\partial r^2} + \frac{1}{S}\frac{\partial^2 p}{\partial z^2}\right) = \delta^2 E^{\frac{1}{2}} \frac{\partial^2}{\partial r^2}\left(\frac{\partial^2 p}{\partial r^2} + \frac{1}{\sigma}\frac{\partial^2 p}{\partial z^2}\right). \tag{A 8}$$

Notice that, for $t = O(1)$, scaling the r variable with $S^{\frac{1}{2}}$ leads to the same equation that results from the same scaling on (2.33), but only if $S \gg \delta E^{\frac{1}{2}}$; for smaller values of S, a different limit equation results from (A 8). Further, even with such an $S^{\frac{1}{2}}$ scaling of the radial coordinate, we notice that scaling t with $S/E^{\frac{1}{2}}$ results in the full equation. Now, the radial diffusion of angular momentum and radial diffusion of density, represented by the final terms in (A 7) are not included in the derivation of §2; therefore, as noted there, the 'long-time' solution given in (2.46a) fails at this timescale.

So, for S smaller than $E^{\frac{1}{2}}$, the appropriate limit equation of (A 8) for times of order unity is just a diffusion equation, in a layer of width $(\delta^2 E^{\frac{1}{2}}/\sigma)^{\frac{1}{2}}$, so long as $\sigma \ll (E^{\frac{1}{2}}/S)^{\frac{1}{2}}$. (For σ much larger than such a value, the width is in act $(E^{\frac{1}{2}}\delta^2 S)^{\frac{1}{4}}$).

At still smaller values of S, the more interior buoyancy layer is still more involved. Though it is the subject of another paper, it is relevant to say here that (A 1) is replaced by the sixth-order system below, once S is as small as $(E\delta^2)^{\frac{2}{3}}/\sigma$,

$$\frac{\partial^6 w}{\partial \eta^6}+\frac{\partial^2 w}{\partial z^2}+\frac{\sigma S}{(E\delta^2)^{\frac{2}{3}}}\frac{\partial^2 w}{\partial \eta^2}=0, \tag{A 9}$$

where $\eta=(r-1)(E\delta^2)^{\frac{1}{3}}$. It is beyond the scope of this paper to explore the detailed solutions of this equation, its matching to outer layers and the core flow; we simply note here the critical value of (small) S for which such a structure arises.

REFERENCES

Benton, E. R. & Clark, A. 1974 Spin up. *Ann. Rev. Fluid Mech.* **6**, 257–280.

Boyer, D. L. & Davies, P. A. 1982 Flow past a circular cylinder on a beta plane. *Phil. Trans. R. Soc. Lond.* A **306**, 533–556.

Buzyna, G. & Veronis, G. 1971 Spin-up of a stratified fluid: theory and experiment. *J. Fluid Mech.* **50**, 579–608.

Davies, P. A. 1972 Experiments on Taylor columns in rotating stratified fluids. *J. Fluid Mech.* **54**, 691–717.

Davies, P. A., Davis, R. G. & Foster, M. R. 1990, Flow past a cylinder in a rotating, stratified fluid. *Phil. Trans. R. Soc. Lond.* A331, 245–286.

Greenspan, H. P. 1968 *The Theory of Rotating Fluids.* Cambridge University Press.

Greenspan, H. P. & Howard, L. N. 1963 On a time-dependent motion of a rotating fluid. *J. Fluid Mech.* **17**, 385–404.

Holton, J. R. 1965 The influence of viscous boundary layers on transient motions in a stratified rotating fluid. Part I. *J. Atmos. Sci.* **22**, 402–411.

Holton, J. R. 1965*b* The influence of viscous boundary layers on transient motions in a stratified rotating fluid. Part II. *J. Atmos. Sci.* **22**, 535–540.

Honji, H., Taneda, S. & Tatsuno, A. 1980 Some practical details of the electrolytic precipitation method of flow visualisation. *Res. Inst. Appl. Mech. Kyushu Univ.* **28**, 83–89.

Hyun, J. M. 1983 Axisymmetric flows in spin-up from rest of a stratified fluid in a cylinder. *Geophys. Astrophys. Fluid Dyn.* **23**, 127–141.

Linden, P. F. 1977 The flow of a stratified fluid in a rotating annulus. *J. Fluid Mech.* **79**, 435–447.

Pedlosky, J. 1967 The spin-up of a stratified fluid. *J. Fluid Mech.* **28**, 463–479.

Pedlosky, J. 1971 Geophysical fluid dynamics. In Mathematical Problems in the Geophysical Sciences (ed. W. H. Reid). Lectures in Applied Mathematics, vol. 13. Providence, RI: Am., Math. Soc.

Pedlosky, J. 1979 *Geophysical Fluid Dynamics.* Springer.

Sakurai, T. 1969 Spin down problems of rotating stratified fluid in thermally-insulated circular cylinders. *J. Fluid Mech.* **37**, 689–699.

Spence, G. S. M. 1986 Studies of baroclinic flows in rotating fluids. Ph.D. dissertation, University of Dundee.

Walin, G. 1969 Some aspects of time-dependent motion of a stratified rotating fluid. *J. Fluid Mech.* 1936, 289–307.

Wedemeyer, E. H. 1964 The unsteady flow with a spinning cylinder. *J. Fluid Mech.* **20**, 383–399.

Weidmann, P. D. 1976*a* On the spin-up and spin-down of a rotating fluid. Part 1. Extending the Wedemeyer model. *J. Fluid Mech.*77, 685–708.

Weidmann, P. D. 1976*b* On the spin-up and spin-down of a rotating fluid. Part 2. Measurements and stability. **77**, 709–725.